Available online at www.sciencedirect.com
ScienceDirect
Acta Materialia 55 (2007) 1573–1587
Acta MATERIALIA
www.actamat-journals.com

Linear analysis of texture–property relationships using process-based representations of Rodrigues space

Veera Sundararaghavan, Nicholas Zabaras *

Materials Process Design and Control Laboratory, Sibley School of Mechanical and Aerospace Engineering, 188 Frank H.T. Rhodes Hall, Cornell University, Ithaca, NY 14853-3801, USA

Received 2 August 2006; received in revised form 25 September 2006; accepted 2 October 2006
Available online 19 December 2006

Abstract

Techniques for exploring texture–property–process relationships in various deformation processes are derived from a reduced-order model of texture evolution. The orientation distribution function (ODF) in polycrystals is represented over the Rodrigues space in a discrete form using finite element interpolation techniques. Linear programming algorithms are developed for retrieving ODFs with extremal or optimal properties from the complete ODF space. The relationship of optimal textures with processing is addressed by representing texture evolution in a space of reduced basis coefficients called the process plane. This involves generation of orthogonal basis functions for representing spatial variations of the ODF in a given process using proper orthogonal decomposition. These basis functions are found to work in interpolatory and extrapolatory processing modes and allow representation of texturing for deviations in the process variables. Optimization problems are posed in the reduced space for retrieving textures with desired properties. A graphical technique is discussed that allows identification of optimal processing paths for reaching desired textures in association with process plane databases.

Keywords: Texture; Materials-by-design; Plasticity; Model reduction

1. Introduction

Realization of optimal material properties is important for hardware components in aerospace, naval and automotive applications where there is a continuous need to reduce material utilization for reduced process cost, fuel consumption and higher mobility. Critical components involve performance indices that are directly related to microstructures obtained during processing. This calls for direct control of microstructure evolution using well-designed processes. Property cross-plots, a standard approach for materials selection, as generalized by Ashby [1], has allowed graphical quantification of property–performance relations. Recent developments in materials-by-design have allowed a more advanced systems approach that integrates processing, structure and property through multi-scale computational material models [2]. In the area of composites, techniques that enable tailoring of microstructure topology have allowed design of structures with interesting extremal properties, such as negative thermal expansion [3] and negative Poisson's ratio [4]. In contrast to composites, techniques that allow tailoring of properties of polycrystalline alloys involve tailoring of preferred orientation of crystals manifested as the crystallographic texture. During forming processes, mechanisms such as crystallographic slip and lattice rotation drive the formation of texture and variability in property distributions in such materials. A useful method for designing materials is through control of deformation processes, leading to the formation of textures that yield desired property distributions.

* Corresponding author. Tel.: +1 607 255 9104; fax: +1 607 255 1222.
E-mail address: zabaras@cornell.edu (N. Zabaras).
URL: http://mpdc.mae.cornell.edu (N. Zabaras).

1359-6454/$30.00
doi:10.1016/j.actamat.2006.10.019

Crystallographic texture is represented using the orientation distribution function (ODF), which describes local densities of crystals over the orientation space. ODFs are defined based on appropriate parameterizations for the crystal lattice rotation, popular representations include Euler-angles [5] and classes of angle-axis representations, the most popular being the Rodrigues parametrization [6]. Conversion of continuous orientation space to finite degrees of freedom for material property optimization require discretization techniques. Most of the discretization schemes developed concentrate on global basis-based representations using spherical harmonics [5,7–9]. An alternate approach presented in Ref. [10,11] represents the ODF using a finite element discretized Rodrigues space with polynomial shape functions defined locally over each element. Using this approach, any ODF is represented through the nodal values of the finite element grid, the dimensionality of the space equal to the number of independent nodes in the ODF discretization. Relationships of textures with properties can be easily constructed in both Fourier and finite element spaces using linear homogenization relationships. Microstructure design techniques aim to invert such relationships so that textures with desired properties are retrieved. Optimization techniques based on linear analysis for addressing this problem were first developed in Ref. [12]. While the work in Ref. [12] involved optimization in the spectral representation space, the first part of the present work establishes the mathematical tools required to perform optimization using the finite element representation. In contrast to the global basis functions used in the spectral representation, finite element shape functions provide local support and are especially useful for capturing sharp textures. Volume-averaged properties are easily computed using finite element quadrature-based integration techniques. The complete set of feasible textures is simply a plane in the space of nodal values (termed 'material plane') while the similar space in the space of spectral coefficients is a more complicated geometrical entity (termed 'material hull' in Refs. [8,9]). While optimization in the complete texture space certainly allows identification of textures with optimal properties, the feasibility of obtaining such textures through processing is still a long-standing problem in microstructure design.

Processing paths of optimal ODFs can be found by searching for optimal textures over a large database of simulated textures from different processing paths. To alleviate the large computational effort involved in construction of such databases, new mathematical models are currently being developed to optimally represent textures from different processing paths. In Ref. [13], this problem was efficiently addressed by representing processing paths as streamline functions in the space of spectral coefficients. This allows inversion of processing paths by tracking streamlines connecting the initial and optimal textures. While the methodology is promising considering that process paths can be described irrespective of the initial texture, the complexity of the model depends on the number of spectral coefficients used to represent texture. Since a large number of spectral terms are needed to capture sharp textural features, complexity of the models used to describe processing paths increases accordingly. In this work, process selection is addressed using reduced representations of ODF evolution similar to those presented in our previous work [14,15]. This involves generation of an optimal orthogonal basis that captures all spatial features of an ODF for a process. Texture evolution paths can be visualized in a low dimensional space of basis coefficients even for sharp textures. A deficiency of the method is that the basis depends on the initial texture and thus requires a database of basis functions covering several different initial textures. However, the basis functions work in extrapolatory modes to represent textures resulting from deviations in the initial texture. This decreases the computational effort involved in construction of processing path databases since a reduced basis constructed from a single simulation is able to capture a number of extrapolatory processing paths.

Texture paths can be represented over simplified geometrical entities called 'process planes' in the reduced space. Optimization techniques are described that allow selection of textures in the 'process plane' that are as close as possible to optimal textures in the 'material plane'. Additionally, low dimensionality of the ODF space from each process mode allows graphical visualization of texture–process–property relationships. This allows selection of processing paths and process parameters for problems using graphical techniques in association with databases of process planes. Examples in this paper are associated with methodologies to achieve extremal or optimal strength and stiffness parameters in face-centered cubic (fcc) copper. The remainder of the paper is organized as follows. In Section 2, representation of fcc texture in Rodrigues space is defined followed by the reduced-order technique for computing texture evolution. In Section 3, we introduce linear programming techniques for obtaining extremal ODFs or desired property distributions from the material plane (i.e. from the space of all possible ODFs without considerations to processing). Section 4 introduces similar design problems in the process plane (i.e. in the space of reduced-order coefficients of a process basis). Section 5 provides an approach for selection of processing paths that realize desired properties. Finally, a summary of the paper and a discussion of limitations and potential extensions are presented in Section 6.

2. Modeling of fcc texture

2.1. Representation in Rodrigues space

The orientation distribution function (ODF) [5,7], the probability density function for orientations, is employed for the quantification of crystallographic texture. Texture evolution methodologies use parameterizations for the crystal lattice rotation which, together with the crystal symmetry, define the problem domain. Angle-axis

representations define an alternative way of representing texture compared with the use of Euler-angles [5,16]. We employ the axis-angle parametrization of the orientation space proposed by Rodrigues [10]. This is based on the unique association of an orientation with a rotation axis and an angle of rotation about that axis. The Rodrigues parametrization is created by scaling the axis of rotation $\mathbf{n}$ as $\boldsymbol{r} = \mathbf{n}\tan(\frac{\theta}{2})$, where θ is the rotation angle. A proper rotation $\mathbf{R}$ relates the lattice orientation to a reference orientation. Given the Rodrigues parametrization $\boldsymbol{r}$, the rotation $\mathbf{R}$ can be obtained as

$$\mathbf{R} = \frac{1}{1+\boldsymbol{r}\cdot\boldsymbol{r}}(\mathbf{I}(1-\boldsymbol{r}\cdot\boldsymbol{r}) + 2(\boldsymbol{r}\otimes\boldsymbol{r} + \mathbf{I}\times\boldsymbol{r})) \tag{1}$$

The fundamental region represents a region of the orientation space such that each crystal orientation is represented uniquely within that space. The fundamental region for the cubic symmetry group results in a truncated cube. The planes that form the faces of the cube are introduced by symmetry rotations about the $\langle 1\,0\,0\rangle$ family of axes and the corners are truncated by planes introduced by rotations about the $\langle 1\,1\,1\rangle$ axes. The ODF (represented by $\mathscr{A}$) describes the local density of crystals over this fundamental region of orientation space. The volume fraction of crystals within a part ($\Re^*$) of the fundamental region is given by $v_f(\Re^*) = \int_{\Re^*}\mathscr{A}\,\mathrm{d}v$. The ODF is normalized to unity over the fundamental region. Here $\mathrm{d}v = \sqrt{\det \boldsymbol{g}}\,\mathrm{d}r_1\,\mathrm{d}r_2\,\mathrm{d}r_3$. Since the orientation space is non-Euclidean, the volume element is scaled by the term $\sqrt{\det \boldsymbol{g}} = \cos^4(\theta/2)$ where $\boldsymbol{g}$ is the metric for the space. If the orientation-dependent property for a single crystal $\chi(\boldsymbol{r},t)$ is known, any polycrystal property can be expressed as an expectation value or average given by:

$$\langle\chi\rangle = \int_{\mathscr{R}}\chi(\boldsymbol{r},t)\mathscr{A}(\boldsymbol{r},t)\,\mathrm{d}v \tag{2}$$

The evolution of ODF is governed by the ODF conservation equation. The conventional Eulerian rate form of the conservation equation is given by [10]:

$$\frac{\partial\mathscr{A}(\boldsymbol{r},t)}{\partial t} + \bigtriangledown\mathscr{A}(\boldsymbol{r},t)\cdot\mathbf{v}(\boldsymbol{r},t) + \mathscr{A}(\boldsymbol{r},t)\bigtriangledown\cdot\mathbf{v}(\boldsymbol{r},t) = 0 \tag{3}$$

where $\mathbf{v}(\boldsymbol{r},t)$ is the Eulerian reorientation velocity. To compute the ODF evolution, the fundamental region is meshed using tetrahedral elements and the evolution equation is solved using a stabilized finite element method [10]. The reorientation velocity in the above equation is evaluated through crystal constitutive relations. In the examples used in the ensuing sections, texturing in fcc materials with 12 $\{1\,1\,1\}\langle 1\,1\,0\rangle$ slip systems is modeled using a rate-dependent viscoplastic Taylor model with material parameters taken from [14].

2.2. Reduced-order model of the ODF

The discussion here follows the work in [14,15] where model reduction of crystal plasticity was first introduced using the technique of proper orthogonal decomposition (POD). Model reduction involves generation of basis functions optimal for representing ODFs obtained from a process path. Using such basis functions, any ODF $\mathscr{A}(\boldsymbol{r},t)$ from the time-history of ODF evolution in a given process can be approximated as follows:

$$\mathscr{A}(\boldsymbol{r},t) = \sum_{m=1}^{b} a_m(t)\phi_m(\boldsymbol{r}) \tag{4}$$

In the above equation ϕ_m represents 'b' basis functions (independent of time) and $a_m(t)$ denotes the corresponding time-dependent coefficients. Once such basis functions ϕ_m are computed, time-dependent coefficients can be used to reconstruct the textures arising from the process path. Readers are referred to Ref. [14] where texture evolution is computed by using Eq. (4) to convert the partial differential equation (Eq. (3)) to an ordinary differential equation. Texture evolution can also be computed across a set of extrapolatory regimes of the process (i.e. conditions deviating from those used to generate the basis functions) using the same set of basis functions.

The 'method of snapshots' is an efficient technique of obtaining basis functions from an ensemble of ODF data $\{\mathscr{A}(\boldsymbol{r},t)\}_{i=1}^{\mathscr{N}}$ consisting of ODFs at various times during texture evolution over a deformation path. Here, the basis functions ϕ take the form [14]:

$$\phi_m = \sum_{i=1}^{\mathscr{N}} u_i^m\mathscr{A}^i \tag{5}$$

where $\mathscr{A}^i$ represent textures from the ensemble and u_i^m is determined by solving the following linear eigenvalue problem:

$$\boldsymbol{C}\boldsymbol{U} = \boldsymbol{\Lambda}\boldsymbol{U} \tag{6}$$

where $\boldsymbol{C}$ is the spatial correlation matrix defined as

$$\boldsymbol{C}_{ij} = \frac{1}{\mathscr{N}}\int_{\mathscr{R}}\mathscr{A}^i(\boldsymbol{r})\mathscr{A}^j(\boldsymbol{r})\,\mathrm{d}v \tag{7}$$

$\boldsymbol{\Lambda}$ and $\boldsymbol{U}$ comprise the eigenvalues and eigenvectors of the system, respectively. To determine a suitable basis size b, one must ensure that the eigen-modes selected capture as much 'system energy' as possible. This is possible by selecting the basis functions that correspond to the largest eigenvalues in $\boldsymbol{\Lambda}$. Once the modes have been evaluated, the optimal basis is generated from Eq. (5). The coefficients $\boldsymbol{a}$ corresponding to any ODF in a deformation path can be retrieved from:

$$a_m = \int_{\mathscr{R}}\mathscr{A}(\boldsymbol{r})\phi_m\,\mathrm{d}v \tag{8}$$

The ODFs in the deformation path follow a curve in the space of reduced coefficients $\boldsymbol{a}$. The success of the technique for representing texture evolution was shown in Ref. [14], where just three basis functions were found to be sufficient for capturing most features of the evolving ODF in any given process. Basis functions are obtained for different processing modes using a 3403 element discretization of

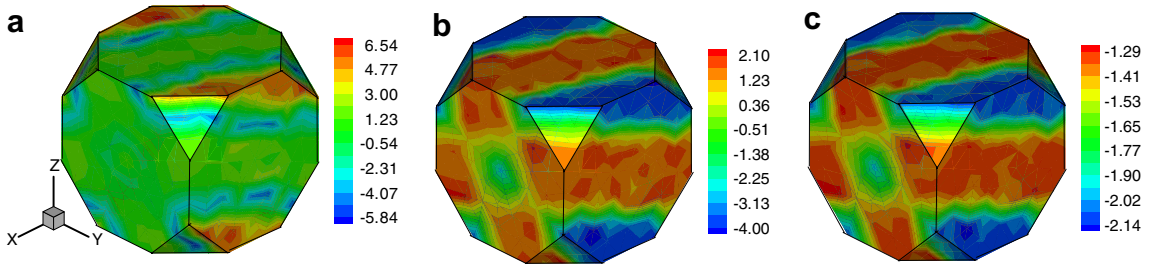

Fig. 1. First three eigen-basis functions for the texture evolution in a tension process from a initial random texture with a strain rate of 1 s^{-1}.

the fundamental region. Basis used in the examples consist of modes generated from an ensemble of data obtained for tension, shear and rolling processes up to time 0.1 s when deformed with a strain rate of 1 s^{-1} using a time step of $\Delta t = 0.01$ s. Fig. 1 shows the three major basis functions of the tension process. The basis depends upon the initial texture $\mathscr{A}(\boldsymbol{r}, t = 0)$ that is used in the solution of ODF evolution (Eq. (3)). However, the strength of POD analysis used here lies in the fact that the reduced basis works in extrapolatory modes to represent texturing under various deviations in the initial texture. As a result, ODFs resulting from processing to a different strain or processing a starting texture that deviates from the one used to build the basis are well approximated using the same set of basis functions. Different basis functions are generated to simulate different process sequences [17]. The reduced modes used to represent the deformation path are different, for example, when modeling tension process on a rolled specimen compared with a process of tension acting on an annealed specimen with random texture.

3. Property representation and optimization in Rodrigues space

Finite element discretization of the orientation space and associated integration schemes using Gauss quadrature allows matrix representation of several properties of the ODF. ODF is assumed to be discretized into N independent nodes with N_{elem} finite elements and N_{int} integration points per element. The constraint that the ODF is normalized to unity over the fundamental region can then be written as

$$\int_{\mathscr{R}} \mathscr{A}\,\mathrm{d}v = \sum_{n=1}^{N_{\text{elem}}} \sum_{m=1}^{N_{\text{int}}} A(\boldsymbol{r}_m) w_m |J_n| \frac{1}{(1 + \boldsymbol{r}_m \cdot \boldsymbol{r}_m)^2} = 1 \tag{9}$$

where $A(\boldsymbol{r}_m)$ is the value of the ODF at the mth integration point with global coordinate $\boldsymbol{r}_m$ of the nth element, $|J_n|$ is the jacobian determinant of the nth element and w_m is the integration weight associated with the mth integration point. This is equivalent to the linear constraint: $\boldsymbol{q}^{\text{int}^{\text{T}}} \boldsymbol{A}^{\text{int}} = 1$, where $q_i^{\text{int}} = w_i |J_i| \frac{1}{(1+r_i \cdot r_i)^2}$ and $A_i^{\text{int}} = A(\boldsymbol{r}_i)$, where each i corresponds to a combination (n,m), $i = 1, \ldots, N_{\text{int}} \times N_{\text{elem}}$. If the orientation-dependent property for a single crystal $\chi(\boldsymbol{r})$ is known, any polycrystal property can be expressed in a linear form as follows:

$$\langle \chi \rangle = \int_{\mathscr{R}} \chi(\boldsymbol{r}) \mathscr{A}(\boldsymbol{r})\,\mathrm{d}v = \sum_{n=1}^{N_{\text{elem}}} \sum_{m=1}^{N_{\text{int}}} \chi(\boldsymbol{r}_m) A(\boldsymbol{r}_m) w_m |J_n| \frac{1}{(1 + \boldsymbol{r}_m \cdot \boldsymbol{r}_m)^2} \tag{10}$$

This is again equivalent to an equation linear in the ODF: $\langle \chi \rangle = \boldsymbol{p}^{\text{int}^{\text{T}}} \boldsymbol{A}^{\text{int}}$, where $p_i^{\text{int}} = \chi(\boldsymbol{r}_i) w_i |J_i| \frac{1}{(1+r_i \cdot r_i)^2}$ and $A_i^{\text{int}} = A(\boldsymbol{r}_i)$, $i = 1, \ldots, N_{\text{int}} \times N_{\text{elem}}$.

An additional constraint in the representation of the material set is the symmetry of the ODF. Orientations on each pair of planes in the fundamental region are equivalent under the symmetries. In the cubic fundamental region, orientations on the $\{1\,0\,0\}$ faces are identified with orientations on the diametrically opposed faces following rotations through $\pi/4$ about the corresponding $\langle 1\,0\,0 \rangle$ axes. Similarly, symmetric orientations on the various $\{1\,1\,1\}$ faces are obtained following rotations through $\pi/3$ about the $\langle 1\,1\,1 \rangle$ axes. The space of ODF values at integration points of the FE mesh does not represent this symmetry. Symmetry conditions are enforced by considering the set of independent nodal points instead of the integration points. Independent nodal points are the reduced set of nodes obtained by accounting for symmetry conditions at the boundaries of the ODF. Let $\boldsymbol{H}$ be the matrix converting the independent nodal values $\boldsymbol{A}^{\text{node}}$ to the integration point values $\boldsymbol{A}^{\text{int}}$ through the shape functions. Then $\boldsymbol{A}^{\text{int}} = \boldsymbol{H}\boldsymbol{A}^{\text{node}}$. The independent nodal values $\boldsymbol{A}^{\text{node}}$ are sufficient to describe the ODF due to the symmetry of the fundamental region. The vector containing the values of the ODF at independent nodal points $\boldsymbol{A}^{\text{node}}$ is hereafter referred to as $\boldsymbol{A}$. The ODF constraint can then be written in terms of the modified $\boldsymbol{q}^{\text{T}} = \boldsymbol{q}^{\text{int}^{\text{T}}} \boldsymbol{H}$ as $\boldsymbol{q}^{\text{T}} \boldsymbol{A} = 1$, $\boldsymbol{A} \geqslant 0$. Properties are specified using the modified $\boldsymbol{p}^{\text{T}} \equiv \boldsymbol{p}^{\text{int}^{\text{T}}} \boldsymbol{H}$ as $\langle \chi \rangle = \boldsymbol{p}^{\text{T}} \boldsymbol{A}$. For calculating more than one property, $\boldsymbol{p}$ is written in a matrix form. The forms of $\boldsymbol{p}$ and $\boldsymbol{q}$ for the design problems addressed in this paper are provided in Appendix A. Another constraint is based on the positivity of the ODF, which constrains the nodal values of the ODF to be positive ($\boldsymbol{A} \geqslant 0$). The space of all possible ODFs thus includes three constraints: normalization, positiveness and symmetry. The constraint $\boldsymbol{q}^{\text{T}} \boldsymbol{A} = 1$, $\boldsymbol{A} \geqslant 0$ means that the complete set of all possible ODFs is a hyperplane in the

space of independent nodal values, which we call the 'material plane'. Optimization to obtain ODFs with extremal properties from this representation is described in the next section.

3.1. Calculation of properties

For the examples in this section, the property matrix $\boldsymbol{p}$ corresponding to polycrystal average properties $[\langle\chi_1\rangle,\ldots,\langle\chi_{n_p}\rangle]$ is generated for calculating the diagonal components of the stiffness matrix and the Taylor factor representing the material strength. The methodologies used for the calculation of these properties are briefly explained here.

1. *Polycrystal stiffness calculation:* Values of elastic parameters for fcc copper crystal are taken as $c_{11} = 168.0$ GPa, $c_{12} = 121.4$ GPa, $c_{44} = 75.4$ GPa. The polycrystal stiffness, $\bar{\boldsymbol{C}}$, is computed through a weighted average (over $\mathscr{A}$) of the stiffness of individual crystals expressed in the sample reference frame. The average values result in the upper bound for the diagonal values of the stiffness matrix.
2. *Yield strength calculation:* The relationship between the macroscopic effective yield strength Y and average slip system hardness τ can be expressed using the Taylor factor M as follows:

$$Y = \sigma_{ij}\frac{\mathrm{d}\epsilon_{ij}}{\mathrm{d}\eta} = M\tau \tag{11}$$

Bishop and Hill analysis is used to determine the stress states (σ_{ij}) for a given deformation in the above equation. Let us apply a deformation to the polycrystal given by the following strain:

$$\mathrm{d}\epsilon = \mathrm{d}\eta\begin{bmatrix}1 & 0 & 0\\ 0 & -0.5 & 0\\ 0 & 0 & -0.5\end{bmatrix} \tag{12}$$

where the principal directions correspond to the rolling direction (RD), the transverse direction (TD) and the normal direction (ND). η can be considered as the absolute amount of the deformation. For a fcc crystal there are 56 stress states which could activate five or more slip systems simultaneously. For a given shape change (here Eq. (12)), the crystal stress state which produces the maximum work is active and the Taylor factor is calculated corresponding to that stress state, from which one can compute the yield stress. More details about this method can be found in Chapter 4 of [18]. To compute the yield stress for different angles to the rolling direction the procedure is the same as above but with applied deformation state (Eq. (12)) rotated by the appropriate angle to the rolling direction. The polycrystal Taylor factor $\langle M\rangle$ can then be determined by averaging using Eq. (2). The random texture value thus computed compares well with the actual value $Y/\tau = 3.067$ for a random polycrystal [18]. Note that the linear relationship provided here computes the strength corresponding to yielding under the particular deformation mode given by Eq. (12) and is not related to either the bounds on yield strength or the uniaxial tensile yield strength. Interested readers are referred to Ref. [19] for the methodology used to compute the upper bound of uniaxial yield strength, in which case, the deformation is varied so that a uniaxial stress state results in the polycrystal.

3.2. Linear programming for property optimization

Linear programming (LP) allows us to address problems involving linear objective function and linear constraints using techniques such as the simplex and the interior point algorithms. General problems that can be solved using linear programming involve a set of equality constraints and a set of inequality constraints as given below [20]:

$$\min_{\boldsymbol{x}} \boldsymbol{f}^{\mathrm{T}}\boldsymbol{x} \text{ such that } \boldsymbol{M}\boldsymbol{x} \leqslant \boldsymbol{m}, \quad \boldsymbol{P}\boldsymbol{x} = \boldsymbol{d}, \quad lb \leqslant \boldsymbol{x} \leqslant ub \tag{13}$$

Sections 3.2.1–3.2.3 pose interesting LP problems for identifying ODFs with extremal or desirable properties and obtaining property closures from the complete ODF space (the 'material plane'). Later sections deal with problems of a similar character using a reduced-order representation, where we emphasize the process selection strategies for obtaining optimal properties.

3.2.1. Identification of textures with extremal properties

Geometrically, linear constraints define a convex polyhedron, which is called the feasible region. Such problems have some interesting properties, including the fact that all local optima are automatically global optima and the optimal solution can only occur at a boundary point of the feasible region. This allows extraction of ODFs with global extrema properties, also called 'extremal ODFs'. The problem of generating extremal ODFs uses $\boldsymbol{x} = \boldsymbol{A}$ as the variable to be identified such that property $\boldsymbol{p}^{\mathrm{T}}\boldsymbol{A}$ is maximized with the constraints that $\boldsymbol{q}^{\mathrm{T}}\boldsymbol{A} = 1$ and $\boldsymbol{A} \geqslant 0$. An example is shown in Fig. 2, where extremal ODFs that maximize a few of the strength and stiffness properties in fcc Cu are provided. As is evident from the plots, extremal ODFs correspond to microstructures with a unique set of orientations (and symmetric equivalents). Extremal ODFs correspond to Dirac delta functions at these orientations. Extremal textures that lead to maximal strength properties are dominated by specific fibers in the orientation space. For example, Fig. 2(a) shows that the ODF for the maximum Taylor factor along the rolling (x-) direction is dominated by the x-axis $\langle 1\,1\,0\rangle$ fiber. Uniaxial compression along the x-axis is a natural way to obtain strong texturing along this fiber to increase the yield strength along the rolling direction. Extremal ODFs are calculated using a mesh with 12096 tetrahedral elements over the orientation space. Note that in examples (a) and (b) in Fig. 2 objectives are defined so as to optimize the Taylor factor calculated along the rolling direction and the transverse direction.

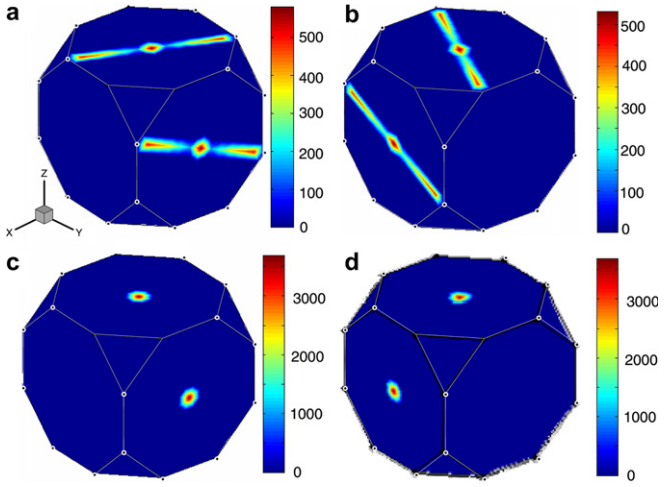

Fig. 2. Extremal ODFs for different properties: (a) ODF for maximum Taylor factor along RD (=3.668), (b) ODF for maximum Taylor factor along TD (=3.668), (c) ODF for maximum C_{44} (=74.923 GPa) and (d) ODF for maximum C_{55} (=74.923 GPa).

3.2.2. Range of properties obtainable from the material plane

Property closures represent the complete range of properties obtainable from the space of the ODFs. These are approximated by the space between the upper and lower bounds of the given property. Upper bound closure of diagonal stiffness values in fcc Cu represents the range of properties obtainable by the upper bound homogenization relation in Section 3. The hull in Fig. 3(a), for example, maps the full range of upper bound values of a combination of diagonal stiffness values. In Section 3.2.1, where we consider extreme points for a single property, the extremal textures were found to correspond to single crystals. A simple technique for constructing property closures (for the homogenization relations considered here) is by establishing the smallest convex region enveloping single crystal property points. Linear programming, although more rigorous, is more intuitive for construction of property closures, since closures are obtained as a result of property maximization or minimization. Connecting faces on the closure may contain polycrystals that are explicitly identified by the LP approach [12]. This approach is also well-suited for other problems posed in this paper, such as identification of textures with desired property combinations (Section 3.2.3) where several properties are optimized simultaneously.

Let v_1, v_2 be the set of properties for which the closure is required. The closure for property v_1 is first found by obtaining the extremal values $(v_{1\max}, v_{1\min})$ as explained in Section 3.2.1. Then, property v_1 is discretized into m values $v_1^i, i = 1, \ldots, m$ between $v_{1\max}$ and $v_{1\min}$. The property closure of the combined set of properties (v_1, v_2) is found by executing a similar extremum LP problem at each point v_1^i with the additional constraint that $\boldsymbol{p}_1^{\mathrm{T}}\boldsymbol{A} = v_1^i$. In general, the closure for a combined set of n properties $(v_1, v_2, \ldots, v_n)$ is an n-dimensional volume found by executing an LP problem extremizing v_n at a set of discrete points $(v_1^i, v_2^j, \ldots, v_{n-1}^l)$ in the closure area of $(v_1, v_2, \ldots, v_{n-1})$. The corresponding LP problem for minimizing v_n is written below:

$$
\begin{aligned}
&\min_{\boldsymbol{A}} v_n = \boldsymbol{p}_n^{\mathrm{T}}\boldsymbol{A} \text{ satisfying the constraints}\\
&\boldsymbol{q}^{\mathrm{T}}\boldsymbol{A} = 1\\
&\boldsymbol{A} \geqslant 0\\
&\boldsymbol{p}_1^{\mathrm{T}}\boldsymbol{A} = v_1^i\\
&\boldsymbol{p}_2^{\mathrm{T}}\boldsymbol{A} = v_{2^j}\\
&\ldots\\
&\boldsymbol{p}_{n-1}^{\mathrm{T}}\boldsymbol{A} = v_{n-1}^l
\end{aligned}
\tag{14}
$$

To maximize v_n another similar problem is executed where the objective is changed as $\min_{\boldsymbol{A}} v_n = -\boldsymbol{p}_n^{\mathrm{T}}\boldsymbol{A}$.

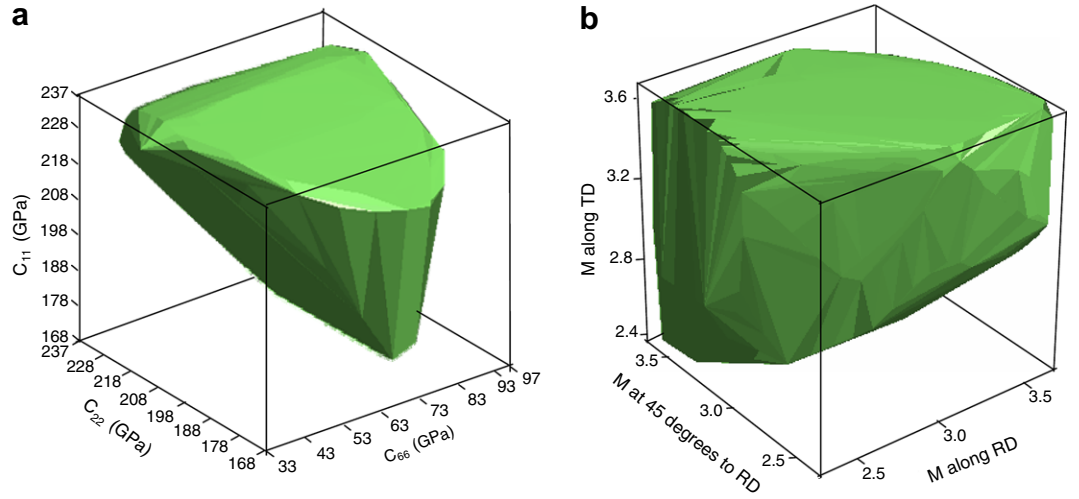

Fig. 3. Space of properties obtainable using the linear homogenization relations in Section 3. (a) The range of combinations of three upper bound stiffness constants $[C_{11}, C_{22}, C_{66}]$. The computed space corresponds to the upper bound property closure for these stiffness constants. (b) The property hull for strength showing all possible combinations of the Taylor factor computed along three directions (RD, 45° to RD and TD).

The full range of Taylor factors is also shown in Fig. 3(b). The closure represents the range of properties obtainable when using the homogenization methodology given in Section 3.

3.2.3. Identification of ODFs with desired distribution of properties

Problems involving identifications of ODFs with the desired combination of several different properties can be performed using the following methodology. The problem is posed as identification of ODF that minimizes the absolute value of error from a desired set of properties, $\min_{\boldsymbol{A}} e_0$, such that $\boldsymbol{p}^{\mathrm{T}}\boldsymbol{A} + \boldsymbol{e} = \boldsymbol{d}$, where $\boldsymbol{d}$ is the desired property set and $\boldsymbol{q}^{\mathrm{T}}\boldsymbol{A} = 1$. Positivity of the ODF dictates the constraint $\boldsymbol{A} \geqslant 0$. We specify a bound $e_0 \geqslant 0$ in the value of the error from a desired property set which is the quantity that is minimized. This additional constraint is defined as $|e_i| \leqslant e_0$, for $i = 1, \ldots, n_p$, where n_p denotes the number of properties to be optimized. This is equivalent to pairs of linear inequalities of the form $-e_i - e_0 \leqslant 0$ and $e_i - e_0 \leqslant 0$. This LP problem uses $\boldsymbol{x} = [e_1, \ldots, e_{n_p}, \boldsymbol{A}, e_0]$ as the variable to be identified. The error e_i is allowed to be of either sign. The constraints are posed by augmenting the $\boldsymbol{p}$ and $\boldsymbol{q}$ matrices (provided in Appendix A) to form the complete linear system of equality constraints.

Although the algorithm highlighted here presents means to identify optimal ODFs on the 'material plane', it does not ensure that such ODFs can be realized through processing. We discuss the reduced basis technique in the next section that allows affiliation of deformation process paths and ODFs with optimal properties.

4. Reduced representation of the ODF for property optimization in deformation processes

The search for optimal ODFs in the 'material plane' did not incorporate any physical aspects of texture evolution. However, the reduced basis technique explained in Section 2.2 allowed representation of texture evolution in a given process using b basis functions ϕ as $A = \sum_{m=1}^{b} a_m \boldsymbol{\phi}_m \geqslant 0$. Any ODF from this processing path was represented completely in the space of coefficients $\boldsymbol{a} = [a_1, \ldots, a_b]^{\mathrm{T}}$. Such a representation allows visualization of textures from any given process in the space of reduced coefficients which we call the 'process plane'. Similar to the constraints in the 'material plane', this space also invokes the positiveness, normalization and symmetry constraints. The normalization constraint in this reduced space is given as $\int_{\mathscr{R}} \sum_{m=1}^{b} a_m \boldsymbol{\phi}_m \, \mathrm{d}v = 1$. Based on this, the equation of the reduced material plane is given as $\sum_{m=1}^{b} a_m \varphi_m = 1$ where $\int_{\mathscr{R}} \boldsymbol{\phi}_m \, \mathrm{d}v = \varphi_m$ with the positiveness constraint $\sum_{m=1}^{b} a_m \phi_m \geqslant 0$. Here, ϕ_m corresponds to the ODF values at the independent nodal locations of the basis. The additional constraint on symmetry that was applied previously for the material plane is not required in the space of reduced-order coefficients since the individual basis functions themselves are periodic and thus symmetry constraints are enforced on any linear combination of this basis.

Process plane representation of an x-axis tension process using basis functions computed from an ensemble of textures obtained by processing a random texture to a strain of 0.1 is shown in Fig. 4(a). Since the constraints are themselves linear, the process plane in Fig. 4(a) is seen as a simple and convex polygon compactly represented close to the origin of the space of reduced coefficients. The process plane is described in a three-dimensional space of reduced-order coefficients $[a_1, a_2, a_3]$. The plane can be conveniently visualized in two dimensions $[a_1, a_2]$ by coloring the points on the plane based on the third dimension a_3. Each point on the process plane in Fig. 4(a) corresponds to an ODF realization. Properties corresponding to these ODFs can be visualized on this plane using color contours on the process plane. Fig. 4(b) shows color contours of the Taylor factor along the rolling direction on the process plane. The third dimension (a_3) is not shown in the property plot since, using Fig. 4(a), the z-coordinate of any point can be retrieved. Figs. 4(c) and (d) show similar process plane representations for the process of x–y shear.

4.1. Processing paths on the process plane

The primary success of proper orthogonal decomposition (POD) is the ability of the reduced basis functions to represent textures arising from various perturbations in conditions used in generating the basis. The robust performance of the basis functions under interpolations and extrapolations of process conditions in particular has found applications in other areas, such as fluid flow simulation and control problems [21–24]. Quantification of the extrapolatory limits of performance of the reduced modes requires extensive experimentation. Indeed, there have been many such studies in different fields (e.g. [25]) devoted to identifying the level of extrapolation that can be accommodated by POD modes within the desired robustness limits. One such study is presented here where we quantify the error in representation of an ODF on the process plane as $100 \times \frac{\|\mathscr{A} - \mathscr{A}^{\mathrm{rec}}\|_2}{\|\mathscr{A}\|_2}$, where $\mathscr{A}$ is the actual ODF resulting from the process (from full-order simulation) and $\mathscr{A}^{\mathrm{rec}}$ is the ODF reconstructed from the coefficients of the reduced-order basis along the path identified in the process plane.

Fig. 5(a) shows a process plane constructed using basis functions generated from an ensemble of textures where an initial random texture is deformed to 0.1 strain under x-axis tension. The ensemble consisted of 10 sets of texture snapshots (obtained at times $\mathscr{T} = \{0.01, 0.02, \ldots, 0.1\}$ s) from crystal plasticity simulation of the process at a strain rate of $1\ \mathrm{s}^{-1}$. The 'process plane' represents all possible ODFs that can be generated using the set of basis functions obtained from this ensemble and represents ODFs from the x-axis tension process for various deviations in strains and initial textures from those used for constructing the ensemble. The ensemble of ODFs used to construct the basis functions are represented as points along the path R–R'

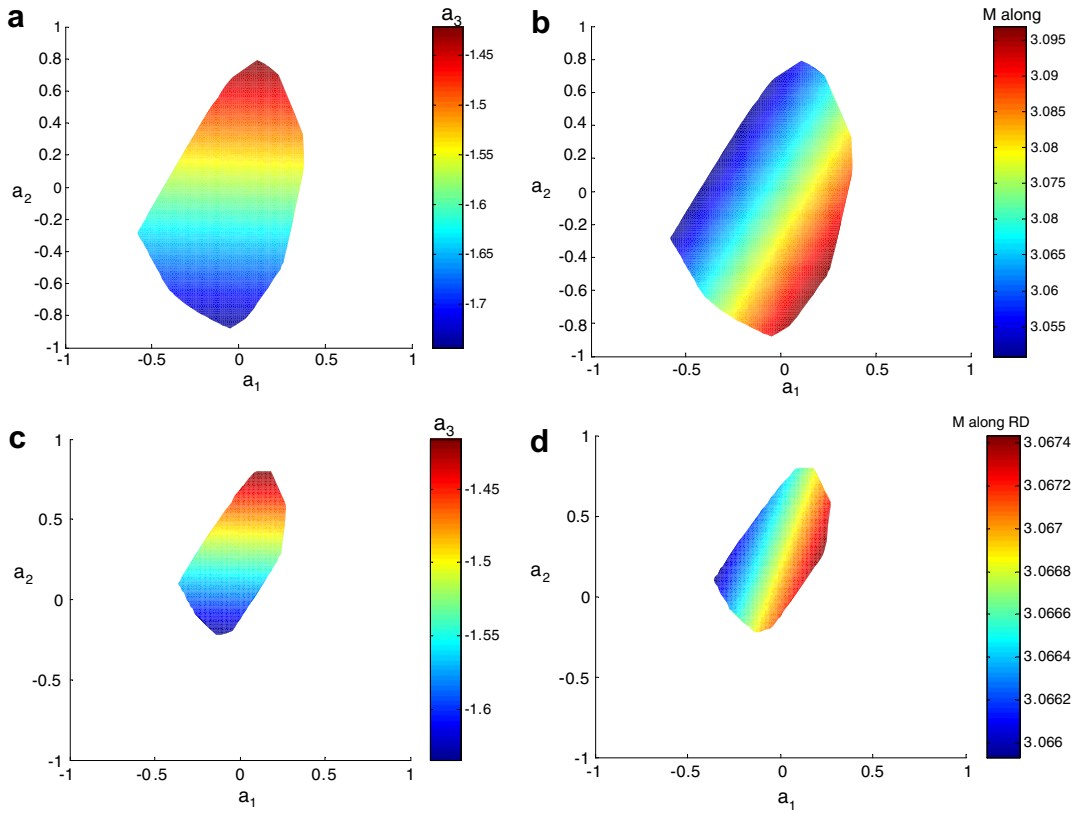

Fig. 4. (a) Process planes for a tension process with a random initial texture. (b) Process plane for tension colored by property (Taylor factor along RD). (c) and (d) Similar process plane representations for shear in the x–y plane.

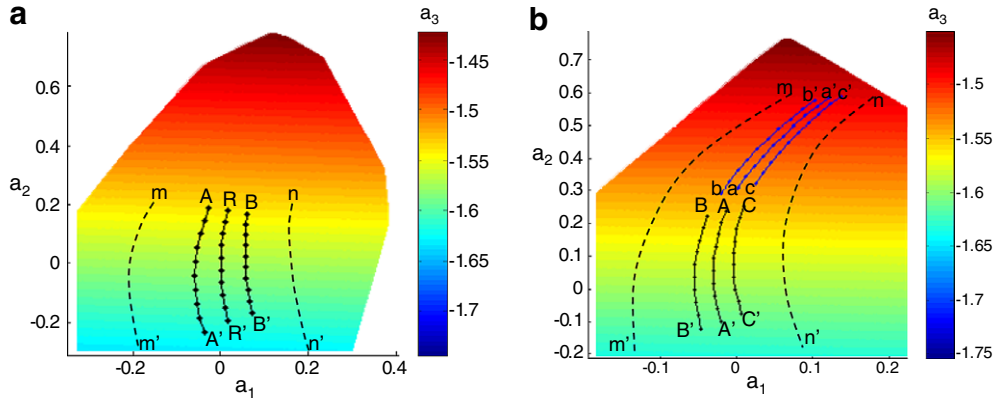

Fig. 5. (a) Process plane for x-axis tension (ensemble obtained by processing an initial random texture to 0.1 strain). Point R corresponds to a random texture, points A and B represent initial textures that deviate from the random texture by 10%. Texture path R–R', A–A' and B–B' are process paths when these initial textures are subjected to x-axis tension up to 0.1 strain. (b) Process plane for x-axis tension process (ensemble obtained by processing the texture obtained by y-axis rolling of a random texture to 0.1 strain to an additional 0.1 strain under x-axis tension). The process paths on the x-axis tension plane for a strain in the y-axis rolling process of 0.1, 0.07 and 0.17 are marked A–A', C–C' and B–B', respectively. Paths a–a', c–c' and b–b' represent the texture paths for x-axis compression to strain of 0.1 with these initial textures. In both figures, m–m' and n–n' delineate the region within which reconstruction of textures from such process paths is at least 90% accurate.

on the process plane. Two different points are chosen on the process plane with ODFs deviating by 10% from the random ODF. These ODFs were subjected to x-axis tension up to 0.1 strain. The different resulting points obtained at times $\mathscr{T}$ in these process paths are depicted on the process plane as curves A–A' and B–B'. The actual ODFs obtained from a crystal plasticity simulation of the process follow a path on the high-dimensional 'material plane' and cannot be easily visualized. It was verified numerically that the points shown on these process paths on the x-axis tension 'process plane' reconstruct the actual ODFs within an error of 2%.

Another example for extrapolatory performance is depicted in a x-axis tension process plane shown in Fig. 5(b). The ensemble from which the basis functions for this process plane was generated also corresponds to snapshots for x-axis tension up to 0.1 strain, but the difference from the earlier example being that the initial texture in this case is obtained from y-axis rolling of a random texture to 0.1 strain. Textures in the ensemble used to generate the basis functions at times $\mathscr{T}$ are represented as points on the curve A–A' in the process plane in Fig. 5(b). We now consider two other process paths where the initial texture for the tension process is changed by varying the strain involved in the rolling process to 0.17 and 0.07. The points in these two process paths computed at times $\mathscr{T}$ are represented with the curves B–B' and C–C', respectively, in the figure. These extrapolatory process paths are within 2% error of the actual ODF paths in the process plane.

The lines m–m' and n–n' at the left and right in Fig. 5(b) delineate the region within which the error in reconstruction of textures in the processing path is less than 10% when compared to textures from a full-order simulation. These curves are generated by comparing actual textures generated from crystal plasticity simulations with textures represented on the process plane when initial textures corresponding to different strains in the y-axis rolling process are deformed in x-axis tension. The curves bound the extrapolation in the initial texture that can be tolerated and follow the process path of these initial textures. This points to the fact that process paths of optimal textures falling within such a region can be predicted with reasonable accuracy. However, process paths traversing points at the far left and right corners of the process plane possess larger errors in reconstruction, and thus the process resulting in these textures cannot be established with confidence. Process selection strategies described later in this work do not incorporate knowledge of inaccessible regions of the process plane. There are situations where an optimal ODF computed could lie in regions (e.g. edges of the process plane) that are inaccessible. An ad hoc way of addressing the problem is to disregard solutions that are close to the edges of the process plane.

In addition to variations in the initial texture, the same basis also works for extrapolations of strains used in constructing the basis. For example, Fig. 5(b) shows the texturing paths (points on these paths computed again at times $\mathscr{T}$) a–a', b–b' and c–c' for x-axis compression to strain of 0.1 with the same initial textures as discussed before, captured within an error of 2%. In principle, it is also possible to construct basis functions using a combined ensemble of textures from different processes in a process sequence. Such basis functions would be able to represent the actual textures (or process path) from all processes in the sequence within a single process plane. The only difficulty with such an approach is that more than three basis functions are required to capture the textures and, consequently, the process planes are not amenable to plotting and visualization.

Naive methodologies for selection of process sequences depend on a large database of computed processing paths requiring a large number of crystal plasticity simulations. Use of process planes for performing process sequence selection is a concept worth pursuing since a process plane constructed from a single simulation captures a number of extrapolatory processing paths. Thus, a search for optimal ODFs over a large set of computed process paths is replaced with a search over a smaller set of process planes. Analysis in the rest of the section introduces methods for identifying process sequences that can be used to reach desired final properties. Once a process sequence is established, existing optimization techniques, such as the gradient based techniques in [14,15,17], can be used to identify parameters such as strain rates for each processing stage. Computational details and key issues in process plane optimization problems are presented in detail in the following sections.

4.2. Identification of ODFs (from a given process) closest to an optimal ODF in the 'material plane'

As described in Section 3.2.3, location of optimal ODFs on the 'material plane' does not convey information on how to realize such ODFs in practice. There may be several processing solutions to this problem. Here, we choose a particular processing path and check if it can closely produce an optimal texture in the material plane. The optimal ODF from the 'material plane' is assumed to be given by a perturbation ($\boldsymbol{r}$) to an ODF in the 'process plane'. We wish to minimize the perturbation from the 'process plane' in some sense such that an ODF from the process plane is as close as possible to the optimal ODF in the material plane.

The optimal ODF is written as $\boldsymbol{A}_{\text{opt}} = \sum_{m=1}^{b} a_m \boldsymbol{\phi}_m + \boldsymbol{r} \geqslant 0$, where $\boldsymbol{A} = \sum_{m=1}^{b} a_m \boldsymbol{\phi}_m$ provides the closest solution in the basis $\boldsymbol{\phi}$ and $\boldsymbol{r}$ is the perturbation (or error) from the optimal ODF. The normalization constraint is given as $\boldsymbol{q}^{\mathrm{T}}\boldsymbol{A}_{\text{opt}} = 1$, and $\boldsymbol{q}^{\mathrm{T}}\boldsymbol{A} = 1$ such that in the LP problem, the former constraint is equivalently specified as $\boldsymbol{q}^{\mathrm{T}}\boldsymbol{r} = 0$. The bound in the value of the solution ODF from the given ODF, $r_0 \geqslant 0$, is minimized. The problem is posed as $\min_{\boldsymbol{a}} r_0$ such that $\boldsymbol{p}^{\mathrm{T}} \sum_{m=1}^{b} a_m \boldsymbol{\phi}_m + \boldsymbol{p}^{\mathrm{T}}\boldsymbol{r} = \boldsymbol{d}$, where $\boldsymbol{d}$ is the desired property distribution. Positivity of the optimal ODF dictates the constraint $\boldsymbol{A} + \boldsymbol{r} \geqslant 0$. In the solution procedure, the basis ($\boldsymbol{\phi}_m$) and the error ($\boldsymbol{r}$) are represented as a vector containing values at independent nodes (set of nodes representing distinct orientations while accounting for crystal symmetries). The ODF in the basis also requires the positivity constraint $\sum_{m=1}^{b} a_m \boldsymbol{\phi}_m \geqslant 0$. The additional constraint on the bound in the value of the solution ODF from the given ODF is defined as $|r_i| \leqslant r_0$, equivalent to pairs of linear inequalities: $-r_i - r_0 \leqslant 0$ and $r_i - r_0 \leqslant 0$, $i = 1, \ldots, N$, where N is the number of independent nodes. This problem uses $\boldsymbol{x} = [r_1, \ldots, r_N, a_1, \ldots, a_b, r_0]^{\mathrm{T}}$ as the variable to be identified. The error (r_i) from the nodal values of the optimal ODF is allowed to be of either sign. Interested readers

are referred to in Appendix B, which provides details on the LP implementation of this problem.

Fig. 6 depicts an example where the problem is to identify the point on a process plane that best represents an optimal ODF in the material plane with desired stiffness properties $\{c_{11} = 210.8575$ GPa, $c_{22} = 210.4191$ GPa, $c_{66} = 66.3110$ GPa$\}$. The basis functions $\{\boldsymbol{\phi}_1, \boldsymbol{\phi}_2, \boldsymbol{\phi}_3\}$ for the process plane considered for this problem were generated from snapshots for x-axis tension up to 0.1 strain of an initial texture that was obtained from y-axis rolling of a random texture to 0.1 strain. The process plane is then constructed from the equation $a_1\varphi_1 + a_2\varphi_2 + a_3\varphi_3 = 1$, where $\varphi_i = \int_V \boldsymbol{\phi}_i \, dv$ with the constraint $a_1\boldsymbol{\phi}_1 + a_2\boldsymbol{\phi}_2 + a_3\boldsymbol{\phi}_3 \geqslant 0$. Texturing during the x-axis tension process for various deviations in strain involved during the y-axis rolling process trace curves (process paths) along this plane as shown by paths 1, 2 in Fig. 6(b) with the initial point being the textures obtained for various perturbations in strains of the y-axis rolling process and rest of the points following the plane dynamics based on the basis functions ($\boldsymbol{\phi}$).

Our objective is to identify the location $\{a_1, a_2, a_3\}$ on the process plane which best represents the optimal ODF on the 'material plane'. Once this location is found, the process path on which the point lies can be identified. The desired stiffness constants and the stiffness constants for the optimal ODF identified in the process plane using the procedure above are compared in Fig. 6(a). The ODF in the material plane that obtains the desired property is shown in Fig. 6(d) but the processing route for this ODF is unknown. The ODF from the process that closely represents this ODF is shown in Fig. 6(c). This ODF is represented by the point A' on the process plane shown in Fig. 6(b). From the fact that the ODF in the process plane closely represents the ODF in the material plane, it is established that the process under consideration is well-suited for achieving the desired set of properties. A possible process path to reach point A' is marked as A–A' in the figure. Location of point A and the strains involved to reach A cannot be obtained in the context of the present analysis and need to be obtained by solving a separate optimization problem such as those presented in [14,15,17]. In such an optimization problem, strain rates of the sequence of processes identified from this analysis (rolling and tension) are incrementally varied from an initial guess so as to minimize the deviation from the optimum texture A' at the end of the process. The strain rates in the ensemble (that generated the basis functions for the process planes) are used as the initial guess. The optimization problem is considerably faster since it solves a reduced-order texture evolution problem at each iteration, utilizing the basis functions already calculated for each process [17]. In this problem, we started by assuming a process sequence that we wanted to work with and then checking whether it can achieve an optimal ODF. In general, this search is repeated over several process planes from a database until a viable solution is found.

4.3. Identification of ODFs (from a given process) to obtain properties closest to a desired set of properties

Similarly to the optimization problem described in Section 4.2, where process plane ODFs closest to optimal ODFs in the material plane were identified, another optimization problem can be posed where the objective is to identify ODFs in the process plane that closely reproduce a desired set of properties. The optimization problem in this case is posed so as to identify ODFs in the process plane whose properties are closest to a desired set of properties in some sense. The objective is to minimize the bound ($e_0 \geqslant 0$) on the absolute value of error from a desired property, $\min_{\boldsymbol{a}} e_0$, such that $\sum_{m=1}^{b} \boldsymbol{p}^{\mathrm{T}} \boldsymbol{\phi}_m a_m + \boldsymbol{p}^{\mathrm{T}} \boldsymbol{e} = \boldsymbol{d}$, where $\boldsymbol{d}$ is the desired set of properties. The normalization constraint is given as $\sum_{m=1}^{b} \boldsymbol{q}^{\mathrm{T}} \phi_m a_m = 1$. Positivity of the ODF dictates the constraint $\sum_{m=1}^{b} \boldsymbol{\phi}_m a_m \geqslant 0$. Bound on, the absolute

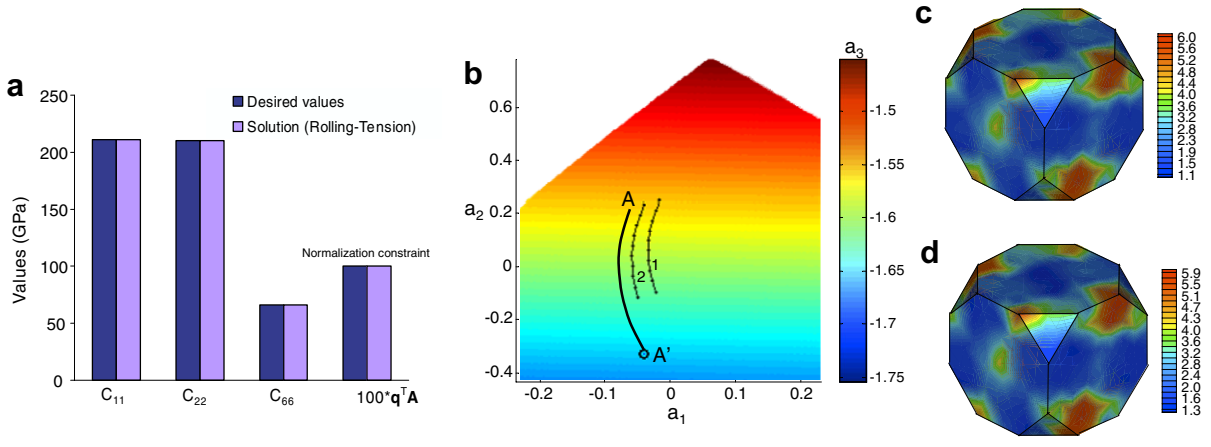

Fig. 6. (a) Desired properties and the closest properties obtainable from the process plane. The last bar shows that the solution ODF is normalized. (b) The optimal point A' is indicated on the process plane along with a possible processing path A–A' leading to it. Processing paths 1, 2 for various different starting textures obtained from different levels of straining in the first (rolling) stage are also shown. (c) Reconstructed optimal ODF from the process plane. (d) Exact ODF that reproduces the desired property.

value of error is defined as $|e_i| \leqslant e_0$. This is equivalent to pairs of linear inequalities, $-e_i - e_0 \leqslant 0$ and $e_i - e_0 \leqslant 0$, where $i = 1, \ldots, n_p$, where n_p denotes the number of properties to be optimized. This problem uses $\boldsymbol{x} = [e_1, \ldots, e_{n_p}, a_1, \ldots, a_b, e_0]^{\mathrm{T}}$ as the variable to be identified. The error e_i is allowed to be of either sign. As an example, for a desired variation of Taylor factor from the rolling to transverse direction shown in Fig. 7(a), the closest property distributions obtainable from the x-axis tension, y-axis rolling and x–y shear process planes are shown. Basis functions for each process was computed from an ensemble of textures obtained by deforming an initial random texture to 0.1 strain with the respective process. As seen in Fig. 7(a), the optimal ODF obtained from the x–y shear process plane fails to reproduce the desired property distribution. The property distribution, however, is represented well by the optimal ODFs identified from the tension or rolling process planes, which are shown in Fig. 7(b) and (c), respectively.

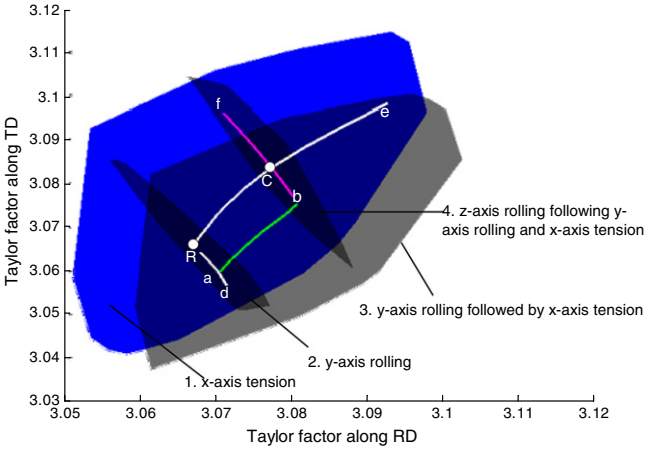

Fig. 8. Property closures of different process planes plotted in the property space for designing process sequences. Two different routes to reach a desired property C from a random ODF (represented at R) are shown. Route R–C follows a x-axis tension process and route R–a–b–C follows a process sequence of y-axis rolling, x-axis tension followed by z-axis rolling.

5. Identification of process paths and optimal ODFs from process–property spaces

Property closures similar to those constructed for the material plane (in Section 3.2.2) can be constructed for visualizing the range of properties obtainable from different process planes. They represent the set of all properties (for a given homogenization method) obtainable from ODFs represented by a process plane. The procedure to obtain extremum properties from the process plane is to pose the LP problem as: $\min_{\boldsymbol{a}} \boldsymbol{f}^{\mathrm{T}}\boldsymbol{a}$ where $f_m = -\boldsymbol{p}^{\mathrm{T}}\boldsymbol{\phi}_m$ for maximizing properties and $f_m = \boldsymbol{p}^{\mathrm{T}}\boldsymbol{\phi}_m$ for minimizing properties, with $m = 1, \ldots, b$. The linear constraint is that the solution ODF is normalized to unity, $\boldsymbol{g}^{\mathrm{T}}\boldsymbol{a} = 1$, where $g_m = \boldsymbol{q}^{\mathrm{T}}\boldsymbol{\phi}_m$, $m = 1, \ldots, b$. Positivity of the ODF dictates that $\sum_{m=1}^{b} \boldsymbol{\phi}_m a_m \geqslant 0$. The procedure for mapping the range of properties obtainable from a process plane is similar to that presented in Section 3.2.2.

The nature of property–process space inherently allows development of several processing routes for obtaining a desired property. Processes can be associated with properties by superimposing the property closures of process planes in the property space. As an example, Fig. 8 shows the property space of Taylor factors along the rolling and transverse directions. Property closures of four different process planes are superimposed in this property space. The process plane for x-axis tension was constructed using basis functions calculated from an ensemble of textures obtained by deforming a random starting texture (R) to a strain of 0.1. Properties for this ensemble fall along path $R - e$ in the figure. Process plane for y-axis rolling was constructed using basis functions calculated from an ensemble of textures obtained by deforming the random texture (R) to a strain of 0.2. Properties for this ensemble fall along path $R - d$ in

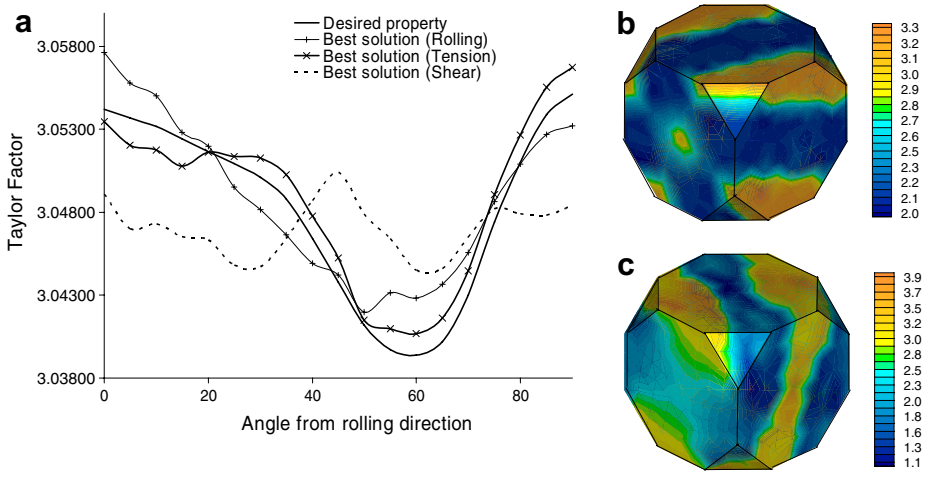

Fig. 7. (a) For a desired property distribution shown, the closest property distributions obtainable in the x-axis tension, rolling and x–y shear process planes are shown. (b) The optimal solution ODF from tension process plane. (c) The optimal solution ODF identified in the rolling process plane.

the figure. A third process plane was constructed using basis functions calculated from an ensemble of textures obtained by y-axis rolling of a random texture up to strain of 0.1 (corresponding to point a) as the starting texture which is processed to an additional 0.1 strain under x-axis tension to end point b. Properties for this ensemble fall along path a–b in the figure. A fourth process plane is constructed using basis functions calculated from an ensemble of textures obtained from z-axis rolling of texture at point b to an additional strain of 0.1. Properties for this ensemble fall along path b–f in the figure. Now, to tailor properties of a random texture (point R – $(3.067, 3.067)$) and reach desired property (point C – $(3.077, 3.084)$), two different process paths can be graphically seen. The simplest route is a direct tension process (path R–C). However, route R–a–b–C is also possible for reaching the desired property. The presence of such a route could have been inferred from the superimposed property closures of process planes shown in Fig. 8 since desired property point C lies on the fourth process plane which involves a process path of the type R–a–b–C.

In association with databases of process planes, such a methodology would be able to identify several process sequences that might lead to a desired property point C starting from a random texture. Once process sequences are identified, the exact process parameters (locations of point a and b) can be found by existing gradient optimization algorithms such as in Ref. [14,15,17] as explained in Section 4.2. To retrieve the optimal ODF (at point C) for the tension process, the property isolines of the Taylor factor in the rolling and transverse direction corresponding to point C are drawn on the property contours of the tension process plane, as shown in Fig. 9(b) and (c), respectively. The intersection point of the iso-property lines in Fig. 9(b) and (c) gives the desired ODF as shown in Fig. 9(d). The graphical solution described here is useful for optimizing up to three properties, which allows visualization of the space. In other cases, where a large number of properties (or a property distribution) need to be optimized, the first step of identifying best processing route needs to be replaced with a linear programming problem of the type used for obtaining desired properties in Fig. 6 or Fig. 7.

5.1. Identification of ODFs with desired nonlinear properties

Properties presented hitherto were linear in the ODF represented by the relationship $\langle \chi \rangle = \boldsymbol{p}^{\mathrm{T}} \boldsymbol{A}$. In the space of

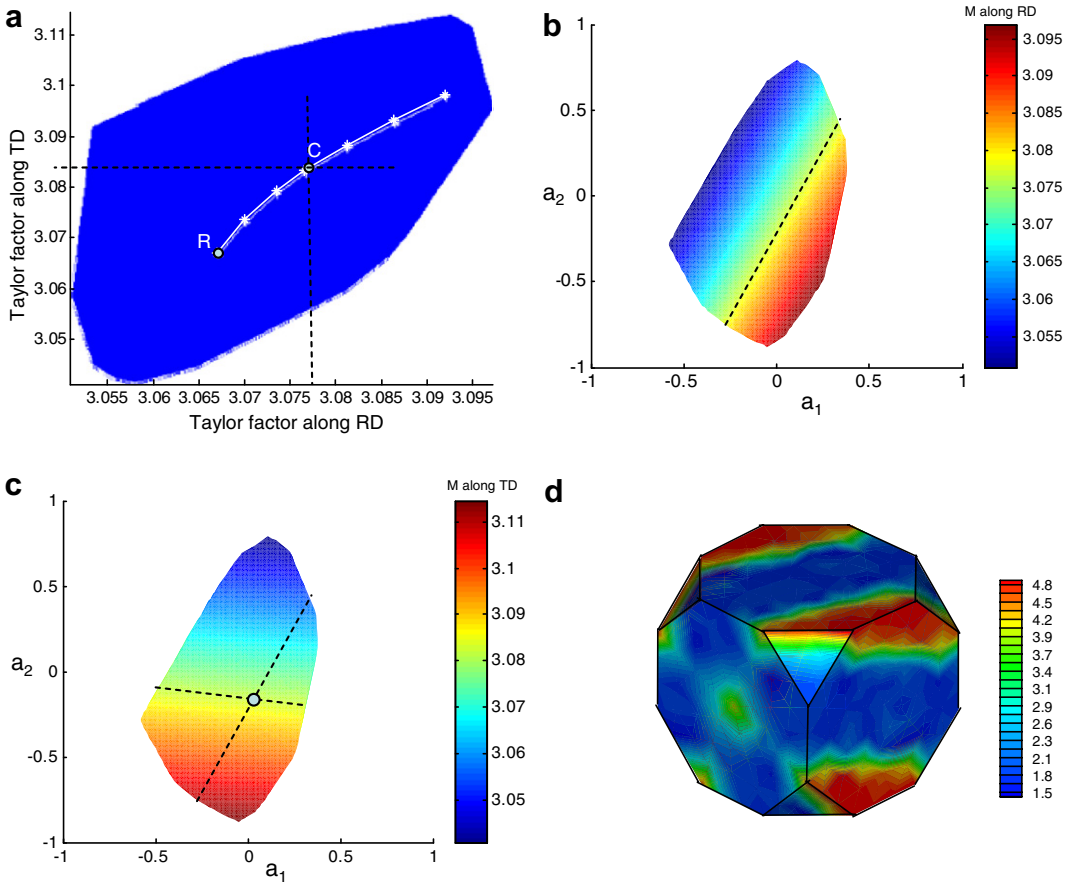

Fig. 9. (a) Property closure for the x-axis tension process with a path leading from property R to C. The ODF corresponding to optimal property C needs to be identified. This is identified from the point of intersection of property iso-lines from the structure–property space shown in (b) and (c). The intersection point of the isolines in plots (b) and (c) gives the desired ODF, as shown in (d).

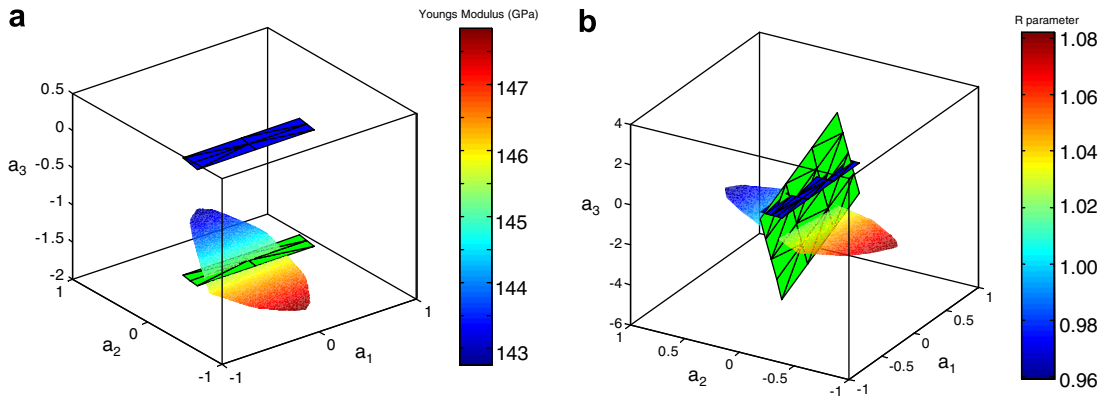

Fig. 10. ODFs with a desired nonlinear property lie on the curve of intersection of iso-property surfaces (for the desired property) with the process plane. The figure shows th eiso-property surfaces for (a) Young's modulus = 143.5 GPa and (b) Lankford R-parameter = 1.023. There are several iso-surfaces in the space of basis coefficients $\{a_1, a_2, a_3\}$ for these two cases, although only one such surface intersects the process plane for x-axis tension.

coefficients of basis functions for a process, iso-property surfaces for linear properties are represented as a family of parallel planes given by $\boldsymbol{p}^{\mathrm{T}}\sum_{m=1}^{3}\boldsymbol{\phi}_m a_m = \langle\chi\rangle$. Iso-property surfaces for nonlinear properties are represented by a nonlinear equation of the form $\langle\chi\rangle = f(a_1, a_2, a_3)$ in the $\{a_1, a_2, a_3\}$ space. Fig. 10(b), for example, represents the iso-property surface for a nonlinear property, the Lankford R-parameter, in the space of reduced-order coefficients of basis functions in an x-axis tension process. The method of computing the R-parameter is presented in Ref. [14]. The basis functions were constructed from an ensemble of textures obtained from processing a random texture to 0.1 strain under x-axis tension. The solution to $R = f(a_1, a_2, a_3) = 1.023$ at 45 to the rolling direction corresponds to two surfaces out of which only one intersects the process plane. Points lying along the curve of intersection of the iso-property surface and the process plane represent valid ODFs in the $\{a_1, a_2, a_3\}$ space with $R = 1.023$. Similar surfaces of the Young's modulus along the rolling direction are plotted in Fig. 10(a). The Young's modulus along the RD is calculated by first inverting the average stiffness matrix found using the approach in Section 3.1 to obtain the average compliance matrix ($\langle\boldsymbol{S}\rangle$). The Young's modulus is then represented as $E = \frac{1}{\langle\boldsymbol{S}\rangle_{11}}$. The solution of $E = 143.5$ GPa corresponds to six surfaces of which only one intersects the process plane. In Fig. 10(a) and (b) the process planes are colored according to the value of the nonlinear property at each point. Although identification of ODFs leading to desired nonlinear properties requires nonlinear optimization techniques [26], a convenient alternative is by visually identifying desired ODFs using such color maps superimposed on process planes. It is interesting to note that the property iso-surface intersecting the process plane is planar in both cases, suggesting that the property may be represented in a linear basis of coefficients as $f(a_1, a_2, a_3) = \sum_{m=1}^{3}\boldsymbol{p}_m^{*\mathrm{T}} a_m = \langle\chi\rangle$ and similar linear programming methodologies as before may be used to invert the property–ODF relationship.

6. Conclusions and future directions

Developments presented here advance materials-by-design for polycrystalline materials through the following new contributions:

- The concept of a 'material plane' in Rodrigues space was employed to construct linear programming solutions to several problems, including identification of optimal or extremal ODFs and the construction of property closures for given linear homogenization relations.
- A new concept of a 'process plane' was established that represents the space of reduced-order coefficients for a given process. The process plane is capable of extrapolating several different processing paths.
- Linear programming methods were constructed to solve problems involving identification of ODFs on the process plane that are as close as possible to desired ODFs on the 'material plane'.
- A graphical solution to the process sequence selection problem was enabled through the identification of process paths on property spaces that represent ranges of properties represented by a process plane.

Selection of optimal textures and processing paths is enabled using databases of reduced-order basis functions and the optimization techniques described in this paper. The shortcomings of the method are related to those of any reduced-order model. The error in reconstruction of process paths increases gradually with increasing extrapolation. This means that processing paths for some parts of the process plane cannot be established accurately. The optimization methodology at present is useful only for linear properties, although studies indicate that iso-property curves of nonlinear properties such as the Lankford R-parameter are almost linear in the process plane. This suggests the possibility that these properties

may be approximated on a linear basis of reduced coefficients. Another restriction is the use of texture representation, which is a first-order feature of the polycrystalline microstructure. Property spaces developed are based on the ODF, which is a lower-order feature of the microstructure that approximates the properties of the real microstructure. Recent developments [27,28] are geared towards design of properties accounting for higher-order features of the microstructure. In summary, future studies should focus on methodologies for constructing a database of process planes, identification of error limits, optimization of nonlinear properties and incorporation of higher-order features of the microstructure in process design.

Acknowledgements

The authors would like to thank the reviewers of the first draft of this paper for providing substantial comments that have helped to improve the technical presentation and focus of this work. The work presented here was funded by the Mechanical Behavior of Materials program (Dr. D. Stepp, program manager) of the Army Research Office (grant W911NF-04-1-0283) and by the Computational Mathematics program (Dr. F. Fahroo, program manager) of the Air Force Office of Scientific Research (grant FA9550-04-1-0070). The work was conducted in our laboratory's Linux cluster and in the super-computing facilities of the Cornell Theory Center.

Appendix A. Formation of property (p) and constraint (q) matrices

Using reduced integration with one integration point per element at a local coordinate of $(0.25, 0.25, 0.25)$ and an integration weight of $w = \frac{1}{6}$, the simplified property matrix $\boldsymbol{p}^{\text{int}}$, corresponding to polycrystal average properties $[\langle\chi_1\rangle, \ldots, \langle\chi_{n_p}\rangle]$ and the normalization constraint vector ($\boldsymbol{q}^{\text{int}}$), are given as

$$\boldsymbol{p}^{\text{int}} = \begin{bmatrix} \frac{1}{6}\chi_1(\boldsymbol{r}_1)|J_1|\frac{1}{(1+r_1\cdot r_1)^2} & \cdots & \frac{1}{6}\chi_{n_p}(\boldsymbol{r}_1)|J_1|\frac{1}{(1+r_1\cdot r_1)^2} \\ \frac{1}{6}\chi_1(\boldsymbol{r}_2)|J_2|\frac{1}{(1+r_2\cdot r_2)^2} & \cdots & \frac{1}{6}\chi_{n_p}(\boldsymbol{r}_2)|J_2|\frac{1}{(1+r_2\cdot r_2)^2} \\ \cdots & & \\ \frac{1}{6}\chi_1(\boldsymbol{r}_{N_{el}})|J_{N_{el}}|\frac{1}{(1+r_{N_{el}}\cdot r_{N_{el}})^2} & \cdots & \frac{1}{6}\chi_{n_p}(\boldsymbol{r}_{N_{el}})|J_{N_{el}}|\frac{1}{(1+r_{N_{el}}\cdot r_{N_{el}})^2} \end{bmatrix}$$

$$\boldsymbol{q}^{\text{int}} = \begin{bmatrix} \frac{1}{6}|J_1|\frac{1}{(1+r_1\cdot r_1)^2} \\ \frac{1}{6}|J_2|\frac{1}{(1+r_2\cdot r_2)^2} \\ \cdots \\ \frac{1}{6}|J_{N_{el}}|\frac{1}{(1+r_{N_{el}}\cdot r_{N_{el}})^2} \end{bmatrix}$$

The $\boldsymbol{H}$ matrix can be defined from the equation $A_e^{\text{int}} = 0.25\sum_{i=1}^{4} A_e^i$, where A_e^{int} is the integration point ODF value at element e and $A_e^i, i = 1, \ldots, 4$ refers to the ODF values at the four nodes of the tetrahedral element e. The $\boldsymbol{p}$ matrix is formed as $\boldsymbol{p} = \boldsymbol{H}^{\text{T}}\boldsymbol{p}^{\text{int}}$ so that any property $\boldsymbol{d}$ can be represented as the scalar product $\boldsymbol{p}^{\text{T}}\boldsymbol{A}$ with the ODF values ($\boldsymbol{A}$) at the independent nodal points.

Appendix B. Formation of augmented system in LP problems

The augmented LP problem for the algorithm in Section 4.2 is presented here. The problem objective is identification of an ODF satisfying given property values ($\boldsymbol{d}$) in the 'material plane' that is closest to a 'process plane'. The equality constraint is specified by three independent equations, as described in Section 4.2:

$$\begin{aligned} &\boldsymbol{p}^{\text{T}}\left(\sum_{m=1}^{b} a_m\phi_m + \boldsymbol{r}\right) = d \\ &\boldsymbol{q}^{\text{T}}\left(\sum_{m=1}^{b} a_m\phi_m\right) = 1 \\ &\boldsymbol{q}^{\text{T}}\boldsymbol{r} = 0. \end{aligned} \tag{15}$$

Three basis functions, ϕ_1, ϕ_2 and ϕ_3, with corresponding coefficients a_1, a_2 and a_3, are used to fully represent the ODFs during a particular process. The unknowns in the LP tableau are then written as $\boldsymbol{x} = [r_1, \ldots, r_N, a_1, a_2, a_3, r_0]^{\text{T}}$. Thus, the augmented system combining the constraints in Eq. (15) can be written as $\boldsymbol{P}_{\text{aug}}\boldsymbol{x} = \boldsymbol{b}$, where $\boldsymbol{b} = [\boldsymbol{d}, 1, 0]^{\text{T}}$ and

$$\boldsymbol{P}_{\text{aug}} = \begin{bmatrix} \boldsymbol{p}^{\text{T}} & \boldsymbol{p}^{\text{T}}\phi_1 & \ldots & \boldsymbol{p}^{\text{T}}\phi_3 & 0 \\ \boldsymbol{0}_{N\times 1}^{\text{T}} & \boldsymbol{q}^{\text{T}}\phi_1 & \ldots & \boldsymbol{q}^{\text{T}}\phi_3 & 0 \\ \boldsymbol{q}^{\text{T}} & 0 & \ldots & 0 & 0 \end{bmatrix}$$

Similar augmentations are performed for the inequality constraints for the problem given as

$$\begin{aligned} &-r_i - r_0 \leqslant 0 \\ &r_i - r_0 \leqslant 0 \\ &\sum_{m=1}^{b} a_m\phi_m + \boldsymbol{r} \geqslant 0 \\ &\sum_{m=1}^{b} a_m\phi_m \geqslant 0 \end{aligned}$$

The augmented system combining the constraints in Eq. (15) can be written as $\boldsymbol{M}_{\text{aug}}\boldsymbol{x} \leqslant \boldsymbol{0}$, where each row of $\boldsymbol{M}_{\text{augmented}}$ *corresponds to the inequalities in Eq. (15), as indicated below:*

$$\boldsymbol{M}_{\text{aug}} = \begin{bmatrix} -\boldsymbol{I}_{N\times N} & \boldsymbol{0}_{N\times 1} & \boldsymbol{0}_{N\times 1} & \boldsymbol{0}_{N\times 1} & -\boldsymbol{1}_{N\times 1} \\ \boldsymbol{I}_{N\times N} & \boldsymbol{0}_{N\times 1} & \boldsymbol{0}_{N\times 1} & \boldsymbol{0}_{N\times 1} & -\boldsymbol{1}_{N\times 1} \\ -\boldsymbol{I}_{N\times N} & -\phi_1 & -\phi_2 & -\phi_3 & \boldsymbol{0}_{N\times 1} \\ -\boldsymbol{0}_{N\times N} & -\phi_1 & -\phi_2 & -\phi_3 & \boldsymbol{0}_{N\times 1} \end{bmatrix}$$

where $\boldsymbol{I}$ is the identity matrix, and the notation $\boldsymbol{1}_{N\times 1}$ and $\boldsymbol{0}_{N\times 1}$ indicates a vector of ones and zeros, respectively, of size $N \times 1$. The objective is to minimize the bound on the error $\boldsymbol{r}$ given by r_0. This objective is given as $\boldsymbol{f}^{\text{T}}\boldsymbol{x}$, where

$$\boldsymbol{f} = [\,\boldsymbol{0}_{1\times N} \quad \boldsymbol{0}_{1\times 3} \quad 1\,]^{\text{T}}$$

Thus, the final LP problem reduces to the solution of the following problem:

$$\min_{\boldsymbol{a}} \boldsymbol{f}^{\mathrm{T}}\boldsymbol{x} \text{ satisfying the constraints}$$

$$\boldsymbol{P}_{\mathrm{aug}}\boldsymbol{x} = \boldsymbol{b}$$

$$\boldsymbol{M}_{\mathrm{aug}}\boldsymbol{x} \leqslant \boldsymbol{0}$$

References

[1] Ashby MF. Materials selection in mechanical design. Tarrytown, NY: Pergamon; 1992.
[2] Olson GB. Science 1997;277(5330):1237–42.
[3] Sigmund O, Torquato S. Appl Phys Lett 1996;69:3203–5.
[4] Lakes R. Deformations in extreme matter. Science 2000;288(5473): 1976–7.
[5] Bunge HJ. Texture analysis in materials science. London: Butterworth; 1982.
[6] Heinz A, Neumann P. Acta Cryst A 1991;47:780–9.
[7] Kocks UF, Tomé CN, Wenk HR. Texture and anisotropy – preferred orientations in polycrystals and their effect on materials properties. Cambridge: Cambridge University Press; 2000.
[8] Adams BL, Henrie A, Henrie B, Lyon M, Kalidindi SR, Garmestani H. J Mech Phys Solids 2001;49:1639–63.
[9] Kalidindi SR, Houskamp JR, Lyons M, Adams BL. Int J Plasticity 2004;20(8–9):1561–75.
[10] Kumar A, Dawson PR. Acta Mater 2000;48:2719–36.
[11] Kumar A, Dawson PR. Comput Meth Appl Mech Eng 1998;153(3-4): 259–302.
[12] Adams BL, Lyon M, Henrie B. Int J Plasticity 2004;20(8-9):1577–602.
[13] Li DS, Garmestani H, Adams BL. Int J Plasticity 2005;21(8): 1591–617.
[14] Acharjee S, Zabaras N. Acta Mater 2003;51(18):5627–46.
[15] Ganapathysubramanian S, Zabaras N. Comput Meth Appl Mech Eng 2004;193:5017–34.
[16] Wenk HR. Preferred orientation in deformed metals and rocks: an introduction to modern texture analysis. London: Academic Press Inc.; 1985.
[17] Sundararaghavan V, Zabaras N. Acta Mater 2005;53/4:1015–27.
[18] Hosford WF. The mechanics of crystals and textured polycrystals. New York: Oxford University Press; 1993.
[19] Proust G, Kalidindi SR. J Mech Phys Solids 2006;54:1744–62.
[20] Luenberger DG. Linear and nonlinear programming. second ed. Norwell, Massachussetts, USA: Kluwer Academic Publishers; 2003.
[21] Peterson JS, SIAM J. Sci Stat Comput 1989;10:777–86.
[22] Ly HV, Trans HT. Math Comput Modell. 2001;33:223–36.
[23] Ravindran SS. Int J Numer Meth Fluids 2000;34:425–48.
[24] Ito K, Ravindran SS. J Comput Phys 1998;143:403–25.
[25] Joyner ML. Appl Math Comput 2006;174(1):732–54.
[26] Lyon M, Adams BL. J Mech Phys Solids 2004;52(11):2569–86.
[27] Adams BL, Gao XC, Kalidindi SR. Acta Mater 2005;53(13): 3563–77.
[28] Sundararaghavan V, Zabaras N. Int J Plasticity 2006;22:1799–824.